Mapping the spatial dynamics of the CD4+ T cell spectrum in classical Hodgkin lymphoma

Victoria Menéndez,¹ José L. Solórzano,^{1,2} Mónica García-Cosío,³ Laura Cereceda,^{1,2} Eva Díaz,¹ Mónica Estévez,⁴ Giovanna Roncador,⁵ Zaira Vega,⁵ Carlos Montalbán,¹ Arutha Kulasinghe,⁶ and Juan F. García ^{1,2}.

- ¹ Translational Research, Fundación MD Anderson International España S.L. Madrid, 28033 Madrid, Spain.
- ² Pathology Department, MD Anderson Cancer Center Madrid. Madrid, Spain.
- ³ Pathology Department, Hospital Universitario Ramón y Cajal. Madrid, Spain.
- ⁴ Hematology Department, MD Anderson Cancer Center Madrid. Madrid, Spain.
- ⁵ Monoclonal Antibodies and Histopathology Units, Spanish National Cancer Research Center (CNIO). Madrid, Spain.
- ⁶ Frazer Institute, Faculty of Medicine, The University of Queensland. Brisbane, Australia.

Running title

Spatial dynamics of CD4+ T cells in cHL

Corresponding author

Juan F. García, Pathology Department, MD Anderson Cancer Center

e-mail: jfgarcia@mdanderson.es

Conflict of interest disclosure

The authors declare no competing financial interests.

Word count:

Abstract: 200 Main text: 4425 1 table and 6 figures. 1 supplementary file.

Mapping the spatial dynamics of the CD4+ T cell spectrum in classical Hodgkin lymphoma

ABSTRACT

As around 25-30% of classical Hodgkin Lymphoma (cHL) patients with advanced stages do not respond to standard therapies, the tumor microenvironment (TME) of cHL is one avenue that may be explored with the aim of improving risk stratification. CD4+ T cells are thought to be one of the main cell types in the TME. However, few immune signatures have been studied, and many of these lack related spatial data. Thus, our aim is to spatially resolve the CD4+ T cell subtypes that influence cHL outcome, depicting new immune signatures or transcriptional patterns that are in crosstalk with the tumor cells. This study was conducted using the Nanostring GeoMx DSP technology, based on the selection of distinct functional areas of patients' tissues followed by the gene-expression profiling. The goals were to assess the differences in CD4+ T cell populations between tumor-rich and immune-predominant areas defined by different CD30 and PD-L1 expression levels and to seek correlations with clinical metadata. Our results depict a complex map of CD4+ T cells with different functions and differentiation states that are enriched at distinct locations, the flux of cytokines and chemokines that could be related to these, and the specific relationships with the clinical outcome.

KEY POINTS

- DSP and cell deconvolution reveal specialized transcriptional dynamics of CD4+ T cells that influence clinical outcomes of cHL patients.
- CD4+ polarization and cytokine gradients differentiate prognostic groups, with immunosuppression proximal to HRS cells in refractory cases.

INTRODUCTION

The tumor microenvironment (TME) has been identified as a key determinant in the pathogenesis, evolution, and treatment sensitivity of many cancer types. One of the most representative models is classical Hodgkin lymphoma (cHL), whose main tissue component comprises an extensive immune cell infiltrate surrounding rare malignant Hodgkin and Reed–Sternberg (HRS) cells. It is notable that HRS cells actively control and remodel the TME, and its constituents influence treatment response. In cHL tumors, the highly abundant CD4+ T cells in the vicinity of tumor cells are considered essential for tumor cell survival but are not completely defined.¹ Indeed, the heterogeneity of CD4+ T cells localized near HRS cells and how this relates to differential clinical outcomes are poorly understood.²

Understanding the spatial distribution of proteins and RNAs has led to discoveries of importance for defining tissue pathology and for elucidating biomarkers that predict patient response to therapy.³ However, there is much still to learn about diagnostics, drug targets, prognostic factors, and biological mechanisms of action determined by protein and RNA localization within tissues. The importance of investigating high-plex expression profiling in a spatially resolved manner has motivated the development of new methodologies like digital spatial profiling (DSP). It allows comprehensive gene-expression analysis in specified regions of interest (ROIs) on formalin-fixed, paraffin-embedded (FFPE) slides, enabling direct mapping of transcriptomic profiles to tissue architecture.³

To address this question, we performed RNA DSP and computational cell deconvolution on FFPE lymph node sections from cHL patients, allowing spatially resolved transcriptomics of CD4+ T cell subpopulations and chemokines in different regions. By multiplex immunofluorescence and segmentation, we selected eight different areas, four belonging to areas in close contact with tumor cells (CD30 > PD-L1 expression) and four from TME areas that do not directly surround HRS cells (CD30 < PD-L1 expression): (1) Active tumor area (CD30-high), where immune cells border the tumor cells that are predominant and express high levels of CD30; (2) Senescent tumor area (CD30-low), where their level of marker expression is low, measuring the immune cells that surround less active and more dispersed cancer cells; (3) Immunosuppressive tumor area (PD-L1-high), where HRS cells and their surroundings express high levels of the immunosuppressive checkpoint molecule PD-L1; (4) Incompetent tumor area (PD-L1-low), where immune cells become located close to HRS cells that do not rely on the overexpression of PD-L1 to facilitate their immune escape; (5) Induced TME (CD30-high) in areas that are close but not directly surrounding the tumor cells; (6) Non-induced TME (CD30-low), in areas located where the tumor cells are not as active or

abundant, and further away; (7) Activated TME (PD-L1-high), in areas overexpressing PD-L1 checkpoint; and (8) Non-activated TME (PD-L1-low), in areas under-expressing PD-L1 checkpoint.

After using the Cancer Transcriptome Atlas (CTA) panel for spatial Gene-Expression Profiling (GEP) in those areas, we computationally deconvolved CD4+ T cells into distinct subpopulations based on their transcription patterns. By registering the locations of CD4+ T cell subsets within selected areas, we identified specialized localization patterns. This revealed pronounced heterogeneity, with follicular T helper cells (Tfhs), regulatory T cells (Tregs), T helper 1 (Th1), Th2 and Th17 cells, among many others, in varying proportions depending on the region and outcome. Most notably, certain T cell subsets accumulated preferentially across active tumor areas, suggestive of recruitment, while others were excluded, hinting at the action of repulsion mechanisms.

This study demonstrates the power of coupling spatially resolved transcriptomics with computational deconvolution to dissect tissue areas. By mapping diverse CD4+ T cell subsets relative to different tumor and TME areas, we gain critical insights into how malignant cells may orchestrate their surroundings through cytokine-dependent recruitment or exclusion, and how PD-L1 expression may influence their behavior. These findings advance our understanding of the unique immunology of cHL and provide a rationale for microenvironment-targeted therapies. In the future, integrated spatial profiling and deconvolution will enable high-resolution immune mapping across malignancies to elucidate therapeutic vulnerabilities.

METHODS

Patient samples

Initially, diagnostic FFPE tumor biopsies and clinical data from 24 cHL patients were obtained from the participating institutions. cHL diagnoses were confirmed by central review using standardized criteria.⁴ To boost the statistical power, cases were intentionally selected to design a balanced series of responders and refractory patients (patients who progress or early relapse).

Additional FFPE samples from reactive lymphoid tissues (2 lymph nodes and 2 tonsil specimens) and 20 cHL tumors were retrieved for independent validation using double immunohistochemistry.

All biospecimens and clinical data were collected with informed patient consent through MD Anderson Foundation Biobank (record number B.0000745, ISCIII National Biobank registry). In accordance with the technical and ethical procedures of the Spanish National Biobank Network,

including anonymization processes in accordance with the Helsinki Declaration. Approval was obtained from the institutional review board (CEIm H. Ramón y Cajal, ref. 445/22).

• Tissue preparation

The 24 FFPE cHL samples were randomly distributed in two tumor microarrays (TMAs) with 12 circular tissue cores each (3 mm in diameter). Duplicate cores of each case were included, totaling 48 cores. (**Figure 1A**). The specific regions within tumors were selected by one of the authors (JFG) to capture tumor-rich areas and to maintain concordance with the histological features of the cases. After quality control, three adjacent slides of 5 μ m thickness were cut from each TMA. The first was H&E stained and two ROIs per patient, one region with high tumor-cell content and the other from a TME-predominant area were pre-selected by a qualified pathologist. The remaining two parallel unstained slides were sent for DSP profiling.

Digital spatial profiling

DSP was performed with the GeoMx digital spatial profiler (NanoString Technologies, Seattle, WA). It enables spatially resolved quantification of RNA abundance in tissue sections. The technique is based on counting unique indexing oligonucleotides that are covalently linked to target-specific mRNA probes.⁵ Each TMA was prepared, linked to a barcoded mRNA probe mix targeting 1800 genes (Cancer Transcriptome Atlas Panel), and stained with fluorescently labeled antibodies (Abs). CD30 was detected using primary anti-CD30 mouse monoclonal Ab (clone CON6D, Spanish National Cancer Center [CNIO]) (diluted at 1:100), plus secondary goat anti-mouse IgG2a conjugated with AF647 (Thermo Fisher) (1:400). PD-L1 was detected using primary anti-PD-L1 rabbit IgG monoclonal Ab (clone EPR19759, Abcam) (10ugr/ml), plus secondary goat anti-rabbit IgG conjugated with AF532 (Thermo Fisher) (1:400). Antibodies were tested to validate the retention of staining specificity after conjugation. Then, duplicated TMAs were scanned to produce fluorescent images that guide the selection of ROIs. Circular ROIs measured 600 µm in diameter per patient were selected by visual assessment of the immunofluorescence of CD30 and PD-L1, two per duplicate: CD30-high, CD30-low, PD-L1-high, and PD-L1-low ROIs. Starting with the same circular regions, we segmented the profiling to directly calculate RNA expression in two separate compartments of the tissue: (1) tumor area including immune cells in direct contact with HRS cells (CD30 > PD-L1 expression) and (2) the surrounding TME (PD-L1 > CD30 expression) (Figure 1B). Double-positive cells are also present in all regions, but with different proportions of CD30 and PD-L1. Finally, TMAs were loaded into the DSP instrument, where UV exposure released indexing oligos from the defined and segmented ROIs. Released oligos were counted by sequencing using the

Illumina Nextseq 2000 platform, allowing spatially mapped quantification of corresponding transcript targets.

Data preparation, normalization, and quality assessment

ROIs were renamed to CD30-high if the CD30 expression level was higher than its overall mean per slide, or CD30-low otherwise. The same criteria were applied to label PD-L1-high and PD-L1-low regions. The resulting count files were analyzed for quality control (QC) using the Bioconductor R package standR (v1.1.5).⁶ Filtering was first conducted to exclude slides and ROIs with poor tissue quality due to poor staining or detachment. The relative log expression (RLE) and principal components analysis (PCA) of the log₂-transformed count per million data were used to assess the overall distribution, to identify any confounding factors arising from the experimental design and to detect the presence of batch effects within the data. To remove unwanted technical variations observed in the RLE analysis, the data were normalized using the trimmed mean of M values (TMM) normalization method in standR (v1.1.5).⁶

Deconvolution analysis

Several gene sets (GSs) were selected from the MSigDB database (https://www.gseamsigdb.org/gsea/msigdb) to encompass all the relevant CD4+ T cell populations, related pathways, and chemokines. Enrichment scores for each GS and patient were computed independently by using the GenePattern single-sample gene-set enrichment analysis (ssGSEA) tool with normalized mRNA data per ROI. Gene expression values for each sample were rank-normalized and an enrichment score was calculated using the Empirical Cumulative Distribution Functions of the genes in the GS and remaining genes. Additionally, normalized bulk gene expression data were used to infer the estimated proportions of infiltrating immune cells using the CIBERSORTx tool (https://cibersortx.stanford.edu/). CIBERSORTx GSs were drawn from gene expression values of the LM22 predefined signature **ImmunoStates Database** matrix, (https://khatrilab.stanford.edu/immunostates/) GSs, from Yu et al.7, and from individual single-cell expression data from healthy humans (GS2 GSE118165, GS3 GSE135390, and GS7 GSE107011). Both deconvolution analyses were randomly permuted 1000 times.

• Double immunohistochemistry

The signature of cytotoxic CD4+ T cells was validated using double immunohistochemistry in FFPE sections from reactive lymph nodes and tonsils, and in an independent series of 20 cHL tumors. Double-labelling was done with a sequential staining method, incorporating monoclonal antibodies for granzyme B (clone GrB-7, Dako, Agilent) or perforin (ab89821, Abcam) as the first antibody,

and CD4 (clone 4B12, Dako, Agilent) as the second antibody. After the primary and secondary antibodies, slides were visualized with EnVision FLEX+ HRP Polymer conjugated with horseradish peroxidase, amplified with Envision Flex Mouse Linker (Dako, Agilent), and developed using 3, 30-diaminobenzidine tetrahydrochloride (FLEX DAB+, Dako, Agilent) or MAGENTA HRP chromogen (GV925, Dako, Agilent). Nuclei were counterstained with hematoxylin. All reactions were performed in an automated immunostaining platform (Autostainer Plus Link, Dako).

Statistical analyses

Comparisons were conducted to identify compartment-specific CD4+ T cell populations, related pathways, and chemokines. Additionally, their associations with patient response groups were examined. All 271 enrichment scores from the ssGSEA and the cell population frequencies from CIBERSORTx were analyzed independently using pipelines developed in R (version 4.2.2, R Foundation for Statistical Computing, Vienna, Austria). When there were several ROIs to be evaluated for each patient and condition, the average of the enrichment scores or cell abundance was calculated before they were statistically analyzed. Cell populations and pathways were then compared independently with respect to areas and disease conditions. Significance was determined using Student's unpaired samples t-tests and Kruskal–Wallis non-parametric tests. All statistical tests were two-sided, and values of p < 0.05 were considered to indicate statistical significance.

RESULTS

• Patient cohort characteristics

The clinic pathological characteristics of the series are summarized in **Table 1**. Staging, assessment of response and patient outcome were defined according to the Lugano criteria.⁸ For statistical comparisons, a patient's outcome was considered favorable (F) when their progression-free survival (PFS) was longer than 2 years; otherwise, the outcome was considered unfavorable (U). All cHL patients were treated with adriamycin-based regimens, mostly ABVD. Ann Arbor Stage and initial treatment response variables were significantly associated with outcome, as expected.

• GeoMx DSP data quality and ROIs

Using the NanoString GeoMx DSP, we investigated the mRNA expression levels of four regions distributed in two FFPE tissue cores for each of the 24 cHL patients (48 cores in total). The tumor and TME compartments were defined by masking the CD30+ PD-L1- and CD30- PD-L1+ regions, respectively, and measured against the CD30 and PD-L1 immunofluorescence-based annotations

(**Figure 1C**). Based on ROI selection and segmentation, eight separate areas were defined, four in tumor-rich areas (CD30 > PD-L1 expression) and the other four in TME regions (CD30 < PD-L1 expression): (1) Active tumor area (CD30-high); (2) Senescent tumor area (CD30-low); (3) Immunosuppressive tumor area (PD-L1-high); (4) Incompetent tumor area (PD-L1-low); (5) Induced TME (CD30-high); (6) Non-induced TME (CD30-low); (7) Activated TME (PD-L1-high); (8) Non-activated TME (PD-L1-low) (**Figure 2A**).

There were no ROIs below the threshold of raw counts (4000), and ROIs with counts of fewer than 100 nuclei were discounted from further analysis (**Supplemental Figure 1**). The expression matrix was evaluated by RLE and PCA plots to identify confounding experimental effects and technical variation. After QC filtering, our dataset retained 113 ROIs from 24 patients with 1142 genes each (**Supplemental figure 2**). In the PCA analysis, the top four principal components explained more than 60% of the expression matrix variation. Normalization was then performed to remove unwanted variation due to the technique, such as library size, while maintaining the biological variance among ROIs (**Figure 2B**).

• Cell deconvolution reveals the complexity of the CD4+ T cell spectrum

ssGSEA was used to estimate the enrichment scores for cell populations and pathways. A GS enrichment score represents the activity level of the biological process in which its members are upregulated or downregulated in a coordinated manner. Unlike with the traditional GSEA tool, we were able to accurately determine the enrichment score for each component and every patient, allowing more powerful statistical analyses to be conducted. Likewise, using CIBERSORTx, we were able to estimate the abundance of distinct CD4+ T cell functional subpopulations, including unexplored specialized cell types, with extraordinary sensitivity, along with related pathways, cytokines, and chemokines.

CD4+ T cells are an important target for studying the tumor microenvironment in cHL for several reasons. The first is that CD4+ T cells are one of the most abundant immune cell types infiltrating the cHL TME.¹ They make up a significant portion of the inflammatory milieu (around 30% of cell counts in our cohort) (**Figure 3**). Secondly, CD4+ T cells directly interact with the malignant HRS cells to form "rosettes", which are a hallmark of Hodgkin lymphoma pathology, suggesting that they have an important functional role.¹⁰ Furthermore, multiple subsets of CD4+ T helper cells like Th1, Th2, Th17, Tregs, etc. have been identified in cHL tumors, indicating that CD4+ T cells are phenotypically and functionally heterogeneous in this setting.¹¹ **Figure 3** illustrates where the 24 different CD4+ T cell subsets deconvoluted with CIBERSORTx are characterized for some representative regions and ROIs. Additionally, the previously established correlation of certain

CD4+ T cell populations with clinical outcomes in cHL,² proves their prognostic relevance and the possibility that CD4+ fingerprints direct the treatment response. Finally, CD4+ T cells secrete cytokines, chemokines, and other factors that are thought to shape the TME and influence HRS cell growth and survival.¹⁰

• CD4+ T cell subsets localize differently between favorable and unfavorable patients

After cell deconvolution, several statistically significant associations between CD4+ T cell populations and cytokines with areas and outcome were identified (**Figure 4**). Some GSs had opposite effects on global survival. For example, exhausted CD4+ T, Th17, and $\gamma\delta$ T cells were unfavorable, while others, like Th1, Th2, and Th9, were favorable (**Figure 4A**). Conversely, cytokines mirrored similar effects, with interleukin 12 (IL-12) and IL-2 as examples of those associated with a favorable prognosis, and IL-17, IL-6, and IL-4 as counterparts (**Supplemental Figure 3**).

Interestingly, cytotoxic CD4+ T cells preferentially accumulated around non-induced TME and active tumor areas, indicative of attraction. This selective tropism focused on active HRS cells is absent from refractory cases, implying a cytotoxic CD4+ T cell deficiency that enables progression. Furthermore, this localization pattern aligns with increased IL-12 and type I IFN expression at the active tumor site in responsive patients, indicative of the stimulation of cytotoxic activity (**Figure 4B**). In active tumor areas, IL-15 and other IFN family members also confer a good prognosis, in contrast to IL-6, IL-21, TGF- β , and several CD4+ T populations, such as central memory CD4+ T cells, effector memory CD4+ T cells, Th1, Th17, Th9, and resting CD4+ T cells. It is of note that other CD4+ T cells are located distally to HRS cells, suggestive of an exclusion mechanism and hinting at differential chemokine effects. Some of those populations are Tr17 cells or CD25+ $\alpha\beta$ T cells that confer a good prognosis in non-activated TME and incompetent tumor areas, together with IFN-responder cells, and chemokines such as IL37 and IFN- γ (**Figure 4C**).

Overall, CD4+ T cells confer a good prognosis, as described before. 12-14 Specifically, they contribute to a beneficial effect when located in the incompetent tumor areas (PD-L1-low) although, strikingly, they are associated with worse outcomes when located in active tumor areas or in induced or activated TME areas (**Figure 5A**). Similarly, other more specific CD4+ T cell subsets, such as central memory CD4+ T cells, behave identically.

Induced TME and activated TME are the areas with the most CD4+ T cell subtypes. Induced TME involves tumor cells educating other immune cell types to be less active against HRS cells. In unfavorable patients, CD4+ T cells and their related pathways are recruited from non-activated TME to induced and activated TME areas. In those areas, CD4+ T cells are activated, with $\alpha\beta$ CD4+

T cells on top. Interleukins like IL-2, IL-37, IL-4, IL-6, tumor growth factor β (TGF- β), tumor necrosis factor (TNF), interferon (IFN), PD1, and CD137 family members are other players that increase in induced TME, where Th17 cells differentiate, and exhausted CD4+ T cells are frequent. T regulatory cells (Tregs) are actively developing in those areas and conferring a bad prognosis, including T regulatory 2 cells, FOXP3+ Tregs, memory Tregs, and naïve Tregs (**Figure 5B**).

Since cytotoxic CD4+ T lymphocytes are poorly described, and we found here a relevant relationship with outcome for this T cell subset (Figure 6A), we considered relevant to validate their presence by double staining in human reactive lymphoid tissue and cHL tumors (Figure 6B). All analyzed samples contained variable amounts of these cells.

• Counterpoised TGF-β and IFN localization gradients differentiate prognostic groups

A striking dichotomy emerged in the spatial patterning of the immunosuppressive cytokine TGF- β compared with interferons. In the activated TME, TGF- β is elevated in responsive cases, while type I, type II IFN, and IFN- γ are selectively upregulated in refractory patients. This differential localization implies type I/II IFN over activation proximal to PD-L1-expressing cells. Conversely, in the induced TME and active tumor area of responsive patients, TGF- β is diminished, while interferons increase in the active tumor site, indicative of localized immune stimulation (**Figure 5C**).

DISCUSSION

The clinical relevance of the immune components of the TME is not a simple, black and white matter, and there is growing evidence of the enormous complexity and plasticity of cell phenotypes. Previous studies using limited immunohistochemistry markers have associated the frequencies of certain immune cell types with cHL clinical outcomes, but without clear clinical applicability, technical standardization, or high interobserver variability. In addition, spatial heterogeneity is also probably an important factor affecting interobserver variability and reproducibility. Thus, a better understanding of TME organization and its functions is essential for identifying refractory patients, and in the search for accurate immune biomarkers. Importantly, recent technological advances now enable high-parameter profiling of immune heterogeneity and spatial relationships within tissues. For example, multiplex *in situ* methods with spectral imaging have emerged that allow the deconvolution of the different elements of the TME. In this study, we applied DSP of cHL tumor sections with the NanoString GeoMx technology and identified specialized localization patterns of CD4+ T cell subsets and related cytokines distinguishing prognostic groups. The global integration of the results allows the simultaneous evaluation of

multiple cell densities/subpopulations as well as the estimation of functional states of immune infiltrates *in situ* and their associations with clinical outcome.

CD4+ T cells are actively recruited by the HRS cells and usually form rosettes surrounding tumor cells, 17,18 which physically interact with HRS cells, providing it with pro-survival signals and shielding it from cytotoxic CD8+ T and NK cells. 11 Recently, Takeuchi *et al.* 19 confirmed the value of DSP in cHL, comparing the gene expression profiles of CD4+ T cell rosettes and other CD4+ T cells separated from the HRS cells. They identified a differential spatial distribution of CD4+ T cells expressing immune checkpoint molecules including OX40, PD-1, and CTLA-4. Although their findings are limited in this single-case study and they could not explore their clinical relevance, they depict the different spatial distributions of immune cells and the relevance of specific functionalities based on location.

Our spatial profiling of CD4+ T cells aligns with and expands on recent research characterizing the cHL TME. Veldman et al. recently characterized and identified exhausted CD4+ T cells expressing TOX and TOX2 transcription factors in the cHL lymph node, but without spatial mapping.¹ In addition, Cader et al. used mass cytometry to contrast tissue samples from primary cHL patients with those of reactive lymph nodes and tonsils.¹¹ Their analysis revealed that Th1-polarized regulatory T cell populations in cHL were expanded compared with normal tissue, along with more differentiated effector CD4+ T cells being skewed towards Th1. Notably, the regulatory T cells exhibited negligible PD-1 expression, unlike the PD-1+ effector Th1 cells. Therefore, differential PD-1 levels combined with immunosuppressive Th1 regulatory T cells may act as complementary mechanisms inducing T cell dysfunction. 10 Also, Alonso-Alvarez et al. found the frequencies of T cell infiltrates to be correlated with outcomes without spatial context.¹² Another recent study by Stewart et al. used multiplexed immunofluorescence and NanoString GeoMx to profile cHL samples.²⁰ They identified stroma-rich niches resembling our immunosuppressive tumor areas, with exhausted CD4+ T cells, versus Tfh-rich regions similar to our non-activated TME associated with favorable outcomes. However, our tumor versus TME segmentation provides greater resolution of the localization patterns. Additionally, our deconvolution quantified distinct CD4+ T cell subsets in each area, revealing the heterogeneity missed by clustering analysis. Furthermore, we linked specialized localization patterns to clinical outcomes, enabling prognostic associations missing from their correlative analysis. Thus, our findings are complementary and extend our previous knowledge.

CD4+ T cells overall conferred a survival benefit when localized distal from CD30 and PD-L1-high areas. However, they were associated with inferior outcomes within the induced and activated TME, as well as in active tumor areas. Unfavorable patients showed trafficking of CD4+ T cells from

non-activated regions into the immunosuppressive tumor milieu, with induction of exhaustion markers like PD-1. Regulatory T cell subsets and cytokines like IL-17, IL-6, and IL-4 were additionally recruited to support immune subversion. In contrast, effector CD4+ T cells were diminished in poor-outcome cases, being relegated only to induced TME, not to active tumor areas. This reveals location-dependent functional polarization, rather than binary categorization of CD4+ T cells as uniformly "anti-tumor" or "pro-tumor".

Intriguingly, cytotoxic CD4+ T cells preferentially accumulated in the active tumor site in favorable prognosis patients (Figure 6A), implying active tropism and HRS-cell targeting. Meanwhile, in refractory cases cytotoxic CD4+ T cells were reduced, indicative of a trafficking deficiency enabling immune escape. CD4+ T lymphocytes with cytotoxic activity are understudied in normal and diseased tissues, with limited evidence available from *in vitro* and murine models.^{21,22} Here we validate the presence of these cells in both human reactive lymphoid tissues and cHL tumors by double staining. The cytotoxic CD4+ T cell pattern aligned with elevated IL-12 and type I interferon expression, suggestive of localized immune stimulation. Thus, the proper positioning and chemokine milieu may enable CD4+ T cell subset anti-tumor functions.

Notably, TGF- β preferentially increased proximal to HRS cells in refractory cases, while, in responsive patients, it localized in PD-L1-high areas. In contrast, type I and II interferons were selectively upregulated in non-activated regions (PD-L1-low) in favorable patients, and close to HRS cells otherwise. This differential localization implies failed TGF- β -mediated activation and dominance of immunosuppression around HRS cells, promoting progression. Overall, these results are in line with previous results from our group (using GEP and cell deconvolution with whole tissues),²³ showing that IFN- γ , TNF, and IL-6 signaling pathways predominated in poor responders whereas the TGF- β pathway was enriched in responders. Here, we complemented these data and expanded the conclusions with spatial information. Hence, the counterpoise between stimulatory and regulatory cytokines underlies outcome distinctions. Integrated analysis of immune topography and cytokine cartography provides a high-resolution perspective.

Clinical development based on immunotherapies targeting the TME has changed the therapeutic paradigm in cHL, mostly relying on the inhibition of PD-1/PD-L1 interaction by anti-PD-1 blockade.^{24,25} The overexpression of PD-1 ligands by the HRS cells is due to frequent copy gains of the 9p24.1 locus, which includes the PD-L1, PD-L2, and JAK2 genes.^{26,27} However, although durable responses to anti-PD-1 treatment have been documented, the majority of patients eventually relapse. Our results may additionally support the use of new targets on the TME.²⁵ One example is CD137 (tumor necrosis factor receptor 9, TNFRSF9, 4-1BB), a glycoprotein receptor that is part of the tumor necrosis factor superfamily. CD137 acts as a T cell co-stimulator, expressed by T cells,

monocytic and dendritic cells, although its expression has also been described in HRS cells.²⁸ CD137 inhibits T-cell activation by eliminating CD137 ligand expression,²⁹ and also induces the secretion of IL-13 by tumor cells, a potent growth factor that polarizes the protective type 1 immune response towards a tumor-supporting type 2 response. Accordingly, treatment effects of 4-1BB agonists in several preclinical mouse models were demonstrated to be important and dependent on CD8+ T cells and NK cells.^{30,31} Importantly, agonists of CD137 have shown great potential for combination therapies with immune checkpoint inhibitors and conventional strategies.³²

Our findings might have additional clinical impact. Another potential target for therapy is IL-6, a pleiotropic lymphokine and a growth factor for normal B cells and plasma cell-derived malignancies. Dysregulated overproduction of IL-6 from germinal center B cells is involved in the pathogenesis of plasma-cell-type Castleman disease.³³ IL-6 signaling is also active in a subset of diffuse large B-cell lymphoma patients with poor prognosis.³⁴ This pathway can be exploited therapeutically using IL-6R or anti-IL-6 monoclonal antibodies that are approved for unrelated indications.^{33,35,36} The HRS cells express IL-6 and the IL-6 receptor,³⁷ and our results confirm that IL-6 and other immunosuppressive cytokines such as IL-4, IL-2, IL-13, and TGF- β are highly enriched in the induced TME. Taken together, it strongly suggests that anti-IL-6/IL-6R drugs may be also an effective treatment for patients with refractory cHL.

This study presents a critical model in which CD4+ T cell localization patterns distinguish refractory cHL patients. We reveal a specific immune topography in poor-outcome cases, with reduced cytotoxic CD4+ T cells in active tumor regions and accumulation of dysfunctional subsets in immunosuppressive niches. This specialized distribution results from failed tropism and aberrant chemokine gradients, allowing immune evasion. Consequently, spatial mapping of CD4+ T cell subsets and functional polarization relative to tumor and TME areas may serve as a predictive biomarker for refractory disease. As immunotherapies continue to proliferate, understanding the influence of localization on CD4+ T cell phenotypes is essential for precision medicine. Our findings provide a rationale for novel diagnostics and rational combination therapies that target immunobiology specific to resistant cHL.

DATA SHARING STATEMENT

GE data are available at GEO and are available from the corresponding author upon reasonable request.

ACKNOWLEDGEMENTS

We thank the MD Anderson Foundation Biobank (record number B.0000745, ISCIII National Biobank Record) for their support for sample and data collection. We also acknowledge the Histopathology Core Unit of the Spanish National Cancer Center (CNIO) for technical support.

This work was supported by Instituto de Salud Carlos III (ISCIII), projects PI19/00083 and PI22/00556 (co-funded by the European Union), and a Roche Foundation Research Grant. V.M. is a recipient of a Predoctoral Grant from ISCIII FIS (PFIS ref. FI20/00184) and the MD Anderson Foundation scholarship for projects in translational oncology 2022.

CONFLICT OF INTEREST DISCLOSURES

The authors declare no competing financial interests.

ETHICS APPROVAL AND CONSENT TO PARTICIPATE

Biospecimens and clinical data were collected with informed patient consent through MD Anderson Foundation Biobank (record number B.0000745, ISCIII National Biobank registry). in accordance with the Helsinki Declaration.

Approval was obtained from the institutional review board (CEIm H. Ramón y Cajal, ref. 445/22).

AUTHORSHIP CONTRIBUTIONS

V.M. performed research, analyzed results, created the figures, and wrote the paper; J.L.S. and E.D. performed research and analyzed results; M.G.-C., L.C., M.E., and C.M. provided samples, clinical data and analyzed results; G.R. and Z.V. performed double immunohistochemically analyses. A.K. contributed to study design, data preparation and collection, and bioinformatics analysis; J.F.G. designed the research, provided funds, analyzed results, and wrote the paper.

REFERENCES

- 1. Veldman J, Rodrigues Plaça J, Chong L, et al. CD4+ T cells in classical Hodgkin lymphoma express exhaustion associated transcription factors TOX and TOX2: Characterizing CD4+ T cells in Hodgkin lymphoma. Oncoimmunology. 2022;11(1):2033433.
- 2. Menéndez V, Solórzano JL, Fernández S, Montalbán C, García JF. The Hodgkin Lymphoma Immune Microenvironment: Turning Bad News into Good. Cancers (Basel). 2022;14(5).
- 3. Hernandez S, Lazcano R, Serrano A, et al. Challenges and Opportunities for Immunoprofiling Using a Spatial High-Plex Technology: The NanoString GeoMx. Front Oncol. 2022;12:890410.
- 4. Alaggio R, Amador C, Anagnostopoulos I, et al. The 5th edition of the World Health Organization Classification of Haematolymphoid Tumours: Lymphoid Neoplasms. Leukemia. 2022;36(7):1720-1748.
- 5. Vandereyken K, Sifrim A, Thienpont B, Voet T. Methods and applications for single-cell and spatial multi-omics. Nat Rev Genet. 2023;24(8):494-515.
- 6. Liu N, Bhuva DD, Mohamed A, et al. standR: spatial transcriptomic analysis for GeoMx DSP data. Nucleic Acids Res. 2024;52(1):e2.
- 7. Yu X, Chen YA, Conejo-Garcia JR, Chung CH, Wang X. Estimation of immune cell content in tumor using single-cell RNA-seq reference data. BMC Cancer. 2019;19(1):715.
- 8. Cheson BD, Fisher RI, Barrington SF, et al. Recommendations for initial evaluation, staging, and response assessment of Hodgkin and non-Hodgkin lymphoma: the Lugano classification. J Clin Oncol. 2014;32(27):3059-68.
- 9. Luo Y, He Z, Liu W, Zhou F, Liu T, Wang G. DTL Is a Prognostic Biomarker and Promotes Bladder Cancer Progression through Regulating the AKT/mTOR axis. Oxid Med Cell Longev. 2022:3369858.
- 10. Calabretta E, d'Amore F, Carlo-Stella C. Immune and Inflammatory Cells of the Tumor Microenvironment Represent Novel Therapeutic Targets in Classical Hodgkin Lymphoma. Int J Mol Sci. 2019;20(21)
- 11. Cader FZ, Schackmann RCJ, Hu X, et al. Mass cytometry of Hodgkin lymphoma reveals a CD4+ regulatory T-cell-rich and exhausted T-effector microenvironment. Blood. 2018;132(8):825-836.

- 12. Alonso-Álvarez S, Vidriales MB, Caballero MD, et al. The number of tumor infiltrating T-cell subsets in lymph nodes from patients with Hodgkin lymphoma is associated with the outcome after first line ABVD therapy. Leuk Lymphoma. 2017;58(5):1144-1152.
- 13. Greaves P, Clear A, Owen A, et al. Defining characteristics of classical Hodgkin lymphoma microenvironment T-helper cells. Blood. 2013;122(16):2856-63.
- 14. Cader FZ, Hu X, Goh WL, et al. A peripheral immune signature of responsiveness to PD-1 blockade in patients with classical Hodgkin lymphoma. Nat Med. 2020;26(9):1468-1479.
- 15. Baghban R, Roshangar L, Jahanban-Esfahlan R, et al. Tumor microenvironment complexity and therapeutic implications at a glance. Cell Commun Signal. 2020;18(1):59.
- 16. Sanchez-Espiridion B, Martin-Moreno AM, Montalban C, et al. Immunohistochemical markers for tumor associated macrophages and survival in advanced classical Hodgkin's lymphoma. Haematologica-the Hematology Journal. 2012;97(7):1080-1084.
- 17. Stuart AE, Williams AR, Habeshaw JA. Rosetting and other reactions of the Reed-Sternberg cell. J Pathol. 1977;122(2):81-90.
- 18. Veldman J, Visser L, Huberts-Kregel M, et al. Rosetting T cells in Hodgkin lymphoma are activated by immunological synapse components HLA class II and CD58. Blood. 2020;136(21):2437-2441.
- 19. Takeuchi M, Miyoshi H, Semba Y, et al. Digital spatial profiling of CD4 in classic Hodgkin lymphoma. Virchows Arch. 2023;483(2):255-260.
- 20. Stewart BJ, Fergie M, Young MD, et al. Spatial and molecular profiling of the mononuclear phagocyte network in classic Hodgkin lymphoma. Blood. 2023;141(19):2343-2358.
- 21. Lancki DW, Hsieh CS, Fitch FW. Mechanisms of lysis by cytotoxic T lymphocyte clones. Lytic activity and gene expression in cloned antigen-specific CD4+ and CD8+ T lymphocytes. J Immunol. 1991;146(9):3242-9.
- 22. Hoek KL, Greer MJ, McClanahan KG, et al. Granzyme B prevents aberrant IL-17 production and intestinal pathogenicity in CD4. Mucosal Immunol. 2021;14(5):1088-1099.
- 23. Menéndez V, Solórzano JL, García-Cosío M, et al. Immune and stromal transcriptional patterns that influence the outcome of classic Hodgkin lymphoma. Sci Rep. 2024;14(1):710.

- 24. Chen R, Zinzani PL, Fanale MA, et al. Phase II Study of the Efficacy and Safety of Pembrolizumab for Relapsed/Refractory Classic Hodgkin Lymphoma. J Clin Oncol. 2017;35(19):2125-2132.
- 25. Armand P, Engert A, Younes A, et al. Nivolumab for Relapsed/Refractory Classic Hodgkin Lymphoma After Failure of Autologous Hematopoietic Cell Transplantation: Extended Follow-Up of the Multicohort Single-Arm Phase II CheckMate 205 Trial. J Clin Oncol. 2018;36(14):1428-1439.
- 26. Green MR, Monti S, Rodig SJ, et al. Integrative analysis reveals selective 9p24.1 amplification, increased PD-1 ligand expression, and further induction via JAK2 in nodular sclerosing Hodgkin lymphoma and primary mediastinal large B-cell lymphoma. Blood. 2010;116(17):3268-77.
- 27. Roemer MG, Advani RH, Ligon AH, et al. PD-L1 and PD-L2 Genetic Alterations Define Classical Hodgkin Lymphoma and Predict Outcome. J Clin Oncol. 2016;34(23):2690-7.
- 28. Anderson MW, Zhao S, Freud AG, et al. CD137 is expressed in follicular dendritic cell tumors and in classical Hodgkin and T-cell lymphomas: diagnostic and therapeutic implications. Am J Pathol. 2012;181(3):795-803.
- 29. Ho WT, Pang WL, Chong SM, et al. Expression of CD137 on Hodgkin and Reed-Sternberg cells inhibits T-cell activation by eliminating CD137 ligand expression. Cancer Res. 2013;73(2):652-61.
- 30. Rajendran S, Ho WT, Schwarz H. CD137 signaling in Hodgkin and Reed-Sternberg cell lines induces IL-13 secretion, immune deviation and enhanced growth. Oncoimmunology. 2016;5(6):e1160188.
- 31. Melero I, Shuford WW, Newby SA, et al. Monoclonal antibodies against the 4-1BB T-cell activation molecule eradicate established tumors. Nat Med. Jun 1997;3(6):682-5. doi:10.1038/nm0697-682
- 32. Müller D. Targeting Co-Stimulatory Receptors of the TNF Superfamily for Cancer Immunotherapy. BioDrugs. Jan 2023;37(1):21-33. doi:10.1007/s40259-022-00573-3
- 33. van Rhee F, Fayad L, Voorhees P, et al. Siltuximab, a novel anti-interleukin-6 monoclonal antibody, for Castleman's disease. J Clin Oncol. 2010;28(23):3701-8.

- 34. Hashwah H, Bertram K, Stirm K, et al. The IL-6 signaling complex is a critical driver, negative prognostic factor, and therapeutic target in diffuse large B-cell lymphoma. EMBO Mol Med. 2019;11(10):e10576.
- 35. Yoshida Y, Tanaka T. Interleukin 6 and rheumatoid arthritis. Biomed Res Int. 2014:698313.
- 36. Yokota S, Imagawa T, Mori M, et al. Efficacy and safety of tocilizumab in patients with systemic-onset juvenile idiopathic arthritis: a randomised, double-blind, placebo-controlled, withdrawal phase III trial. Lancet. 2008;371(9617):998-1006.
- 37. Tesch H, Jücker M, Klein S, et al. Hodgkin and Reed-Sternberg cells express interleukin 6 and interleukin 6 receptors. Leuk Lymphoma. 1992;7(4):297-303.

TABLES

Table 1. Summary of clinical data for all classical Hodgkin Lymphoma patients. A chi-squared test was used to determine the significance of associations between categories of the clinical variables and the outcome. NS = nodular sclerosis; MC = mixed cellularity; IPS = International Prognostic Score; EBV = Epstein–Barr virus; CR = complete remission; PD = progressive disease; PR = partial response; Favorable = PFS > 2 years; Unfavorable = PFS \leq 2 years; n.s. = non-significant.

	Total	Unfavorable	Favorable	p
Age (years)				
≥ 65	3 (13%)	3 (100%)	0 (0%)	n.s.
< 65	21 (87%)	9 (43%)	12 (57%)	
Gender				
Male	13 (54%)	6 (46%)	7 (54%)	n.s.
Female	11 (46%)	5 (46%)	6 (54%)	
cHL subtype				
NS	15 (63%)	7 (47%)	8 (53%)	n.s.
MC	9 (37%)	5 (56%)	4 (44%)	
Ann Arbor stage				
IV	9 (37%)	7 (78%)	2 (22%)	0.035
I-III	15 (63%)	5 (33%)	10 (67%)	
IPS				
≥ 3	4 (17%)	4 (100%)	0 (0%)	n.s.
< 3	20 (83%)	8 (40%)	12 (60%)	
EBV infection				
Positive	5 (21%)	3 (60%)	2 (40%)	n.s.
Negative	17 (71%)	8 (47%)	9 (53%)	
No data	2 (8%)	1 (50%)	1 (50%)	
Response to first treatment				
CR	16 (%)	4 (25%)	12 (75%)	< 0.001
PR + PD	8 (%)	8 (100%)	0 (0%)	

FIGURE LEGENDS

Figure 1. Experimental design. (A) Schematic representation of tumor microarray (TMA) construction. 12 tissue cores of cHL patients were placed on each slide. Parallel cuts were H&E-stained to pre-select areas of interest with high and low tumor-cell content. (B) Diagram of regions of interest (ROIs) selected by CD30 and PD-L1 levels and subsequent segmentation. (C) Real immunofluorescence image of a representative section inside an ROI, showing how the mask recognizes staining even at the single-cell level.

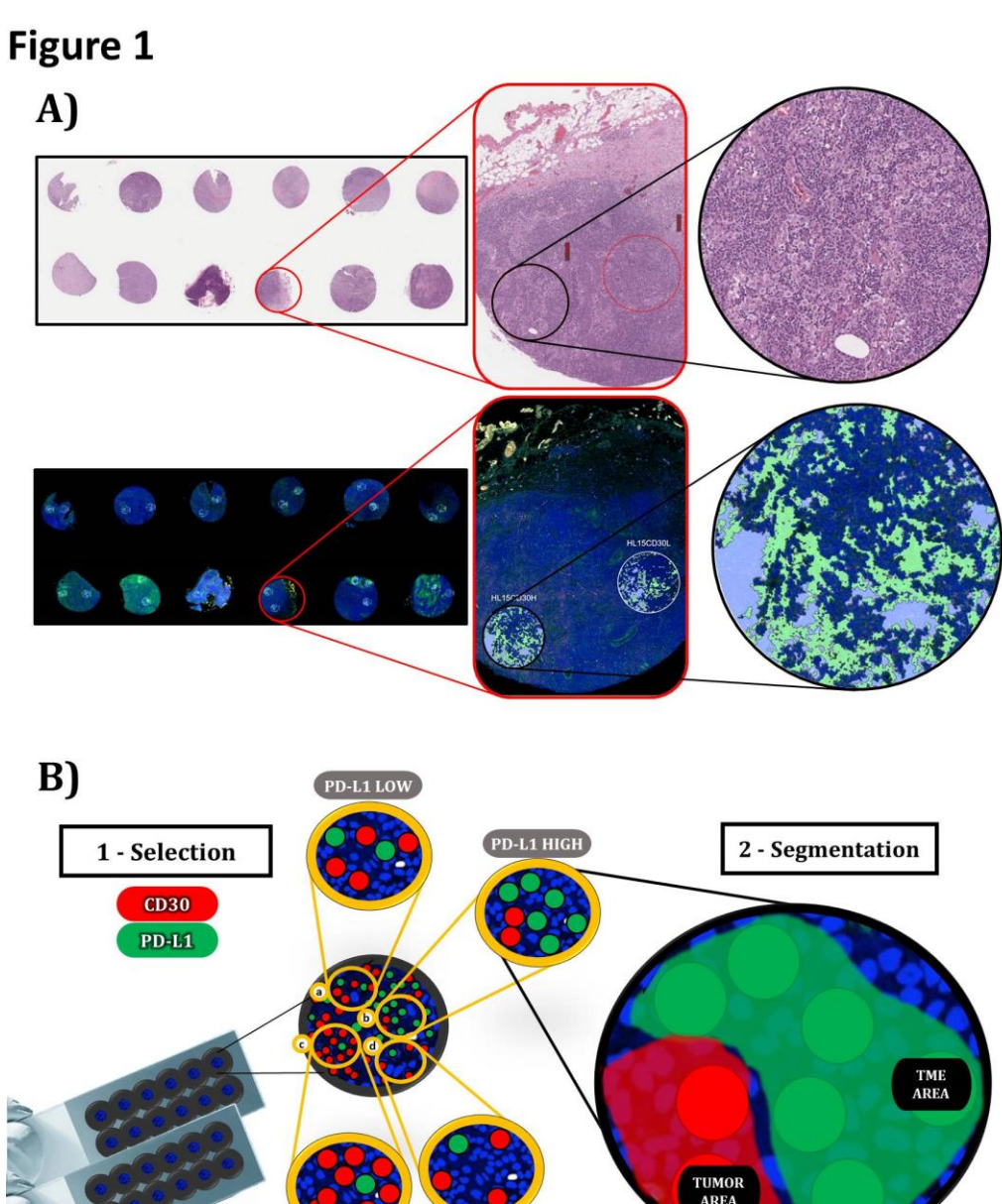
Figure 2. Spatial phenotyping of cHL tumor samples. (A) Tissue compartmentalization was performed by masking CD30+ PD-L1- (Tumor) and CD30- PD-L1+ (TME) areas. The morphology markers included CD30 (red) for tumor cells, PD-L1 (green) for immune cells, and Syto 13 (blue) for the nucleus. Tumor segmentation on regions of interest (ROIs) was done to capture tumor masks (light blue) and TME regions (green). Masks were created using the CD30+/- and PD-L1+/-features to liberate barcodes for digital counting by the NanoString nCounter platform. (B) Principal component (PC) analysis after normalization of the spatial transcriptomic data. This apportions the variability of biological factors and represents it as PC1 and PC2. Some of the most relevant genes are represented, coinciding with important drivers of cHL.

Figure 3. CD4+ T cells account for around 30% of total cell content. Representation of cHL patient fingerprints in the induced microenvironment (TME) and active tumor areas by CIBERSORTx cell abundance in regions of interest that remained after quality-control filtering. The analysis included 24 CD4+ T cell phenotypes, whose distribution can be seen among patients. F = Favorable. U = Unfavorable.

Figure 4. Localization and association with outcome. Tissue compartmentalization with only significant variables (p < 0.05). (A). CD4+ T cell subpopulations associated with an unfavorable prognosis are shown in red. Those associated with good outcomes are shown in green. Otherwise, they are preferentially localized in the compartment without any association with outcome. Some variables were associated with favorable prognosis regardless of the specific area (green box) or with unfavorable outcomes (red box). (B) Gradient of chemokines and cytokines from active tumor areas to induced and non-induced tumor microenvironment (TME) compared between favorable and unfavorable patients. (C) PD-L1 expression affects the chemokine distribution in the TME and tumor areas differently in responders and refractory patients. U = unfavorable. E = V

Figure 5. Plasticity of CD4+ T cell subsets and chemokines among areas driving different outcomes. (A) CD4+ T cells in refractory patients are less abundant in incompetent tumor areas and more numerous in active tumor areas and in induced TME. (B) Unfavorable patients present strong activation of the PD1 pathway in the active tumor areas, more exhausted CD4+ T cells in their induced TMEs, and greater numbers of Tregs in their active tumor areas. (C) IFN-I and TGF- β 1 are examples of the opposing roles of TGF and IFN in the active tumor area of cHL. Additionally, TGF- β 2 is enriched in patients with poorer outcomes in the induced TME compartment.

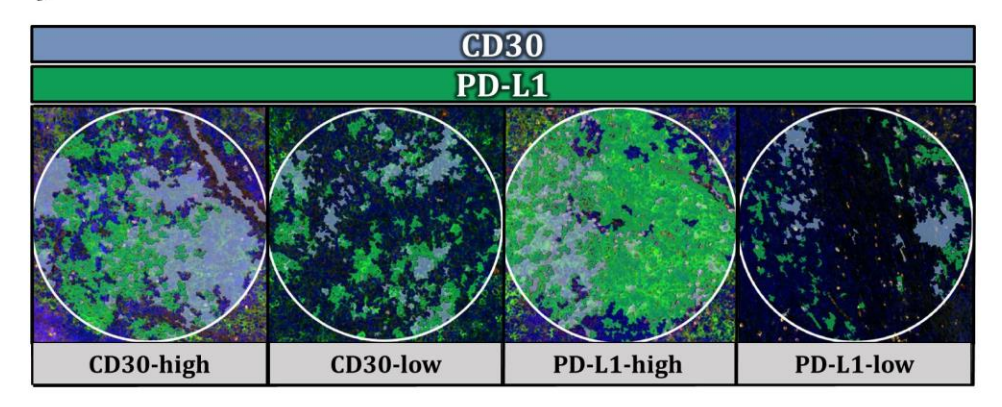
Figure 6. Cytotoxic CD4+ T cells. (A) Cytotoxic CD4+ T cells are more abundant in Favorable patients in active tumor areas (p value = 0.043). (B) Photomicrographs using double immunohistochemistry show cytotoxic CD4+ cells in reactive lymph node (upper panel) and Hodgkin lymphoma (lower panel). Inset: detail of double positive cells. Simultaneous staining using red chromogen for CD4 and brown chromogen for granzyme B and perforin.



CD30 HIGH 24 patients FITC/525nm: SYTO 13: DNA (Blue) Cy3/568nm: Alexa 532: Custom: PD-L1 (Green) Cy5/666nm: Cy5: Custom: CD30 (Red) C)

Figure 2

A)



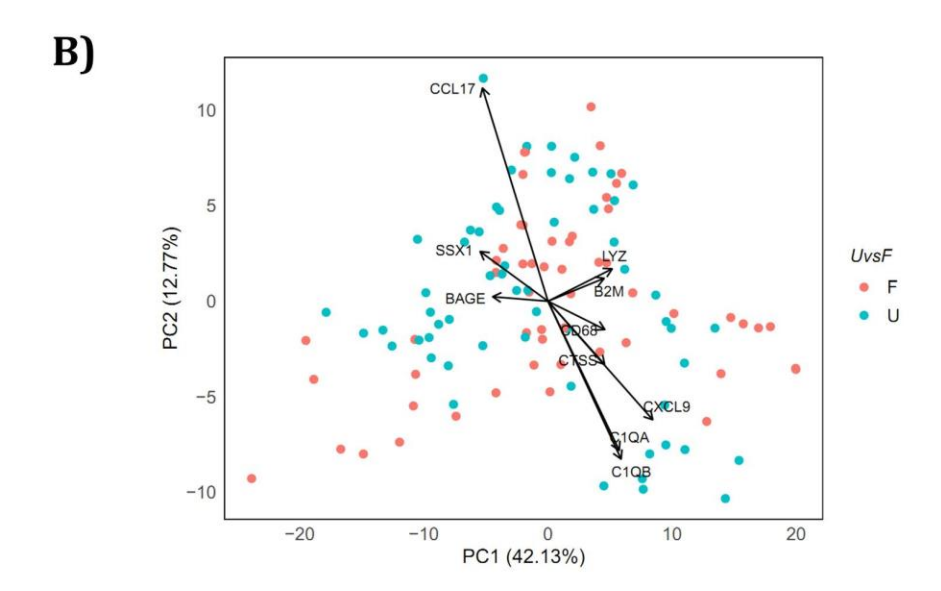


Figure 3

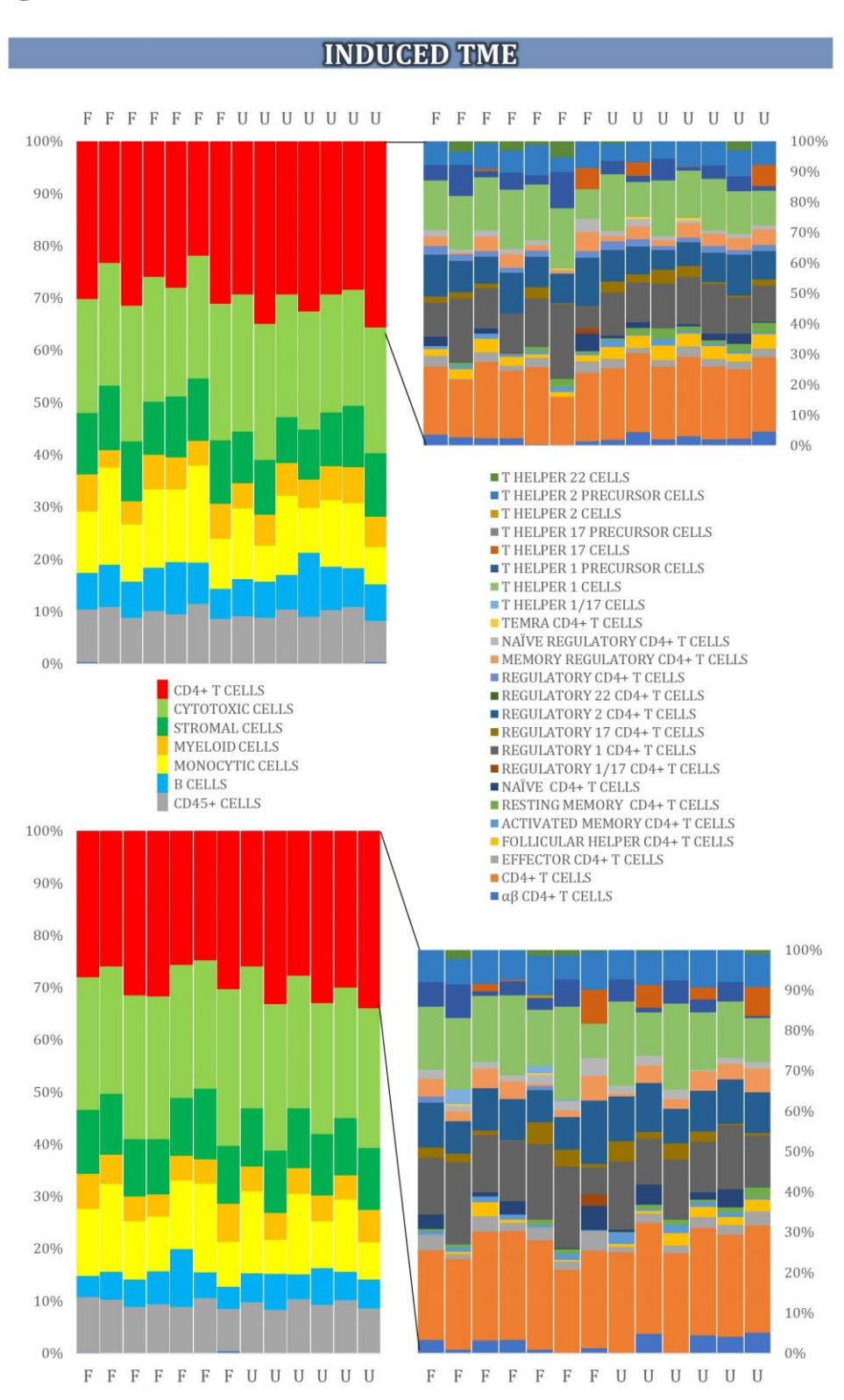


Figure 4

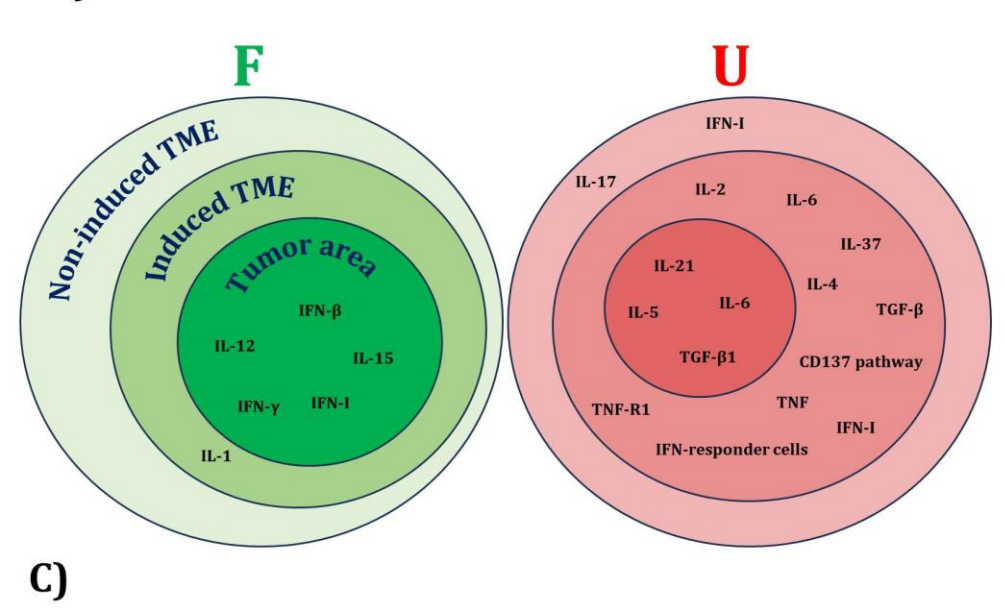
/	۱	7	١
r	۱		ı
-		-	į

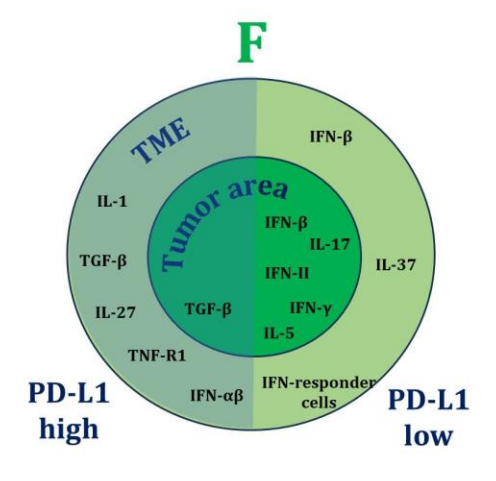
PDL1+ (TME)

CD4+ T cells Effector CD4+ T cell activation Central memory CD4+ T cells Tfh cells	Effector memory CD4+T cells Tregs Naïve Tregs Th1 cells	Treg development Treg differentiation Th2 cells Th9 cells	Th2 cytokine production	
Exhausted CD4+ T cells	Gammadelta CD4+ T cells	Th17 cells		
CD30 HIGH	CD30 LOW	PDL1 HIGH	PDL1 LOW	
Activated CD+ Naive CD+T COSI COSI COSI COSI COSI COSI COSI COSI	Activated CD4+T cells Cytotoxic CD4+T cells Effector memory PD1+ CD4+T cells Gammadelta CD4+T cells Treg development	Activated Central Tregs GH+ T-cells memory CH+ Memory Tregs CD++ T-cells Tfl cells CD++ T-cells Tfl cells CD++ T-cells Activated Tal 7 cells Activation Tri cells The CD++ T-cells CD++ T-cell Tri cells CD++ T-cells CD++ T	Activated CD4+ T Effector memory cells CD4+ T cells Alphabeta CD2+ T recolls Effects of T recolls CD4+ T cells T cells Naive CD4+ T cells T cells T recolls T recoll	
INDUCED TME	NON-INDUCED TME	ACTIVATED TME	NON-ACTIVATED TME	
CD4+ T-clib Central memory CD4+ Thi Crelis Central memory CD4+ Thi Crelis Control CD4+ T-clis Control CD4+ T-clis Thi can Thi call differentiation Thi can Thi call differentiation differentiation differentiation cells Tregs Tregs Tregs Triggian Tregs Triggian Trig	Effector CD4+ T cells Tr2 cells Gammadelta CD4+ T cells Naïve Tregs Th17 cells Th2 precursors	CD28+CD4+T cells Tfh cells Exhausted CD4+ T cells Tregs Th t cells Th 1 precursors Th17 cells Th2 cells Type II immune response	Activated CD4+ T cells CD4+ T cells CD4+ T cells Naive CD4+ T cells Effector memory CD4+ T cells Alphabeta CD25+ CD4+ T cell differentiation Tregs Th1 cells TD17 cells	
ACTIVE TUMOR AREA	SENESCENT TUMOR AREA	IMMUNOSUPPRESSIVE TUMOR AREA	INCOMPETENT TUMOR AREA	

B)

CD30+ (TUMOR AREA)





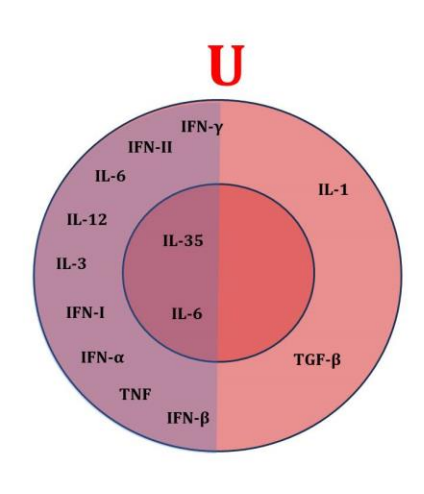


Figure 5

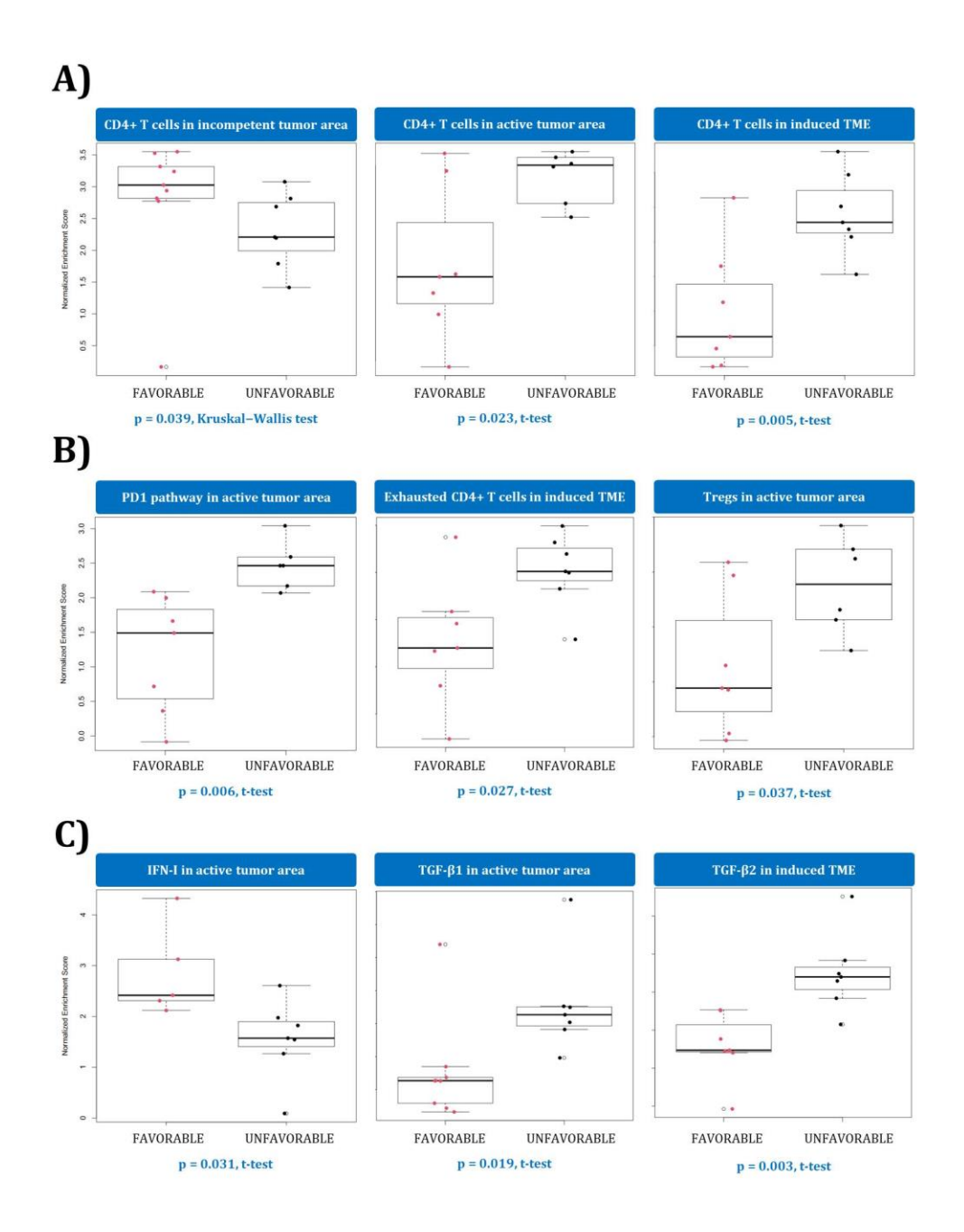
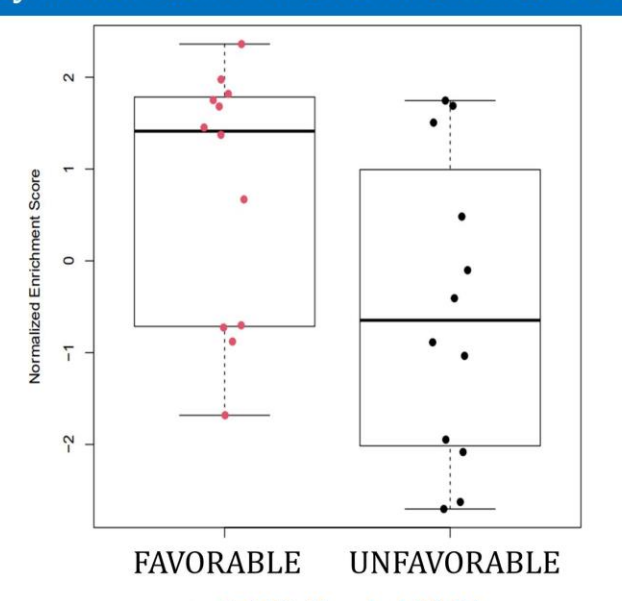


Figure 6



Cytotoxic CD4+ cells in active tumor area



p = 0.043, Kruskal-Wallis

